Renewable Energy 119 (2018) 834–843

Contents lists available at ScienceDirect

Renewable Energy

journal homepage: www.elsevier.com/locate/renene

From bioethanol exploitation to high grade hydrogen generation: Steam reforming promoted by a Co-Pt catalyst in a Pd-based membrane reactor

Adolfo Iulianelli [a, *], Vincenzo Palma [b], Giuseppe Bagnato [a], Concetta Ruocco [b], Yan Huang [c], Nejat T. Veziroğlu [d], Angelo Basile [a, **]

[a] Institute on Membrane Technology of the Italian National Research Council (CNR-ITM), via P. Bucci Cubo 17/C c/o University of Calabria, Rende, CS 87036, Italy
[b] Department of Industrial Engineering, University of Salerno, Via Giovanni Paolo II 132, Fisciano, SA 84084, Italy
[c] State Key Laboratory of Materials-oriented Chemical Engineering, College of Chemical Engineering, Nanjing Tech University, Xin-Mo-Fan Road 5, Nanjing 210009, China
[d] International Association for Hydrogen Energy, 5794 SW 40 St. #303, Miami, FL 33155, USA

ARTICLE INFO

Article history:
Received 17 July 2017
Received in revised form
10 October 2017
Accepted 15 October 2017
Available online 21 October 2017

Keywords:
Bioethanol
Hydrogen
Pd-based membrane reactor
Steam reforming

ABSTRACT

There is a general agreement about the consideration that the fossil fuels are a limited resource and the emission of carbon dioxide and other harmful products are the main cause of the global warming and climate change. The interest for decreasing the fossil fuels dependence and reducing the greenhouse gases emissions represents a top priority. The biomass is a renewable resource useful for biodiesel and bioethanol production. The latter, most plentiful, is currently considered as green ethanol produced from biomass by biological processes. Meanwhile, membrane reactors represent an innovative and intensified technology for the production and the simultaneous recovery of high-grade hydrogen in only one stage. Here, we describe an efficient medium-temperature (T = 400 °C) bioethanol steam reforming process in a thin (~5 μm of metallic layer) supported Pd-based membrane reactor packed with a not commercial Co(10%)Pt (3%)/CeO_2-ZrO_2-Al_2O_3 bi-metallic catalyst at space velocity between 1900 h^{-1} and 4800 h^{-1} and reaction pressure between 1.5 and 2.0 bar. A real bioethanol mixture coming from industry is supplied to the membrane reactor for producing high grade hydrogen, reaching 60% of ethanol conversion (versus ~ 40% of the equivalent conventional reactor) at 400 °C, 2.0 bar and 1900 h^{-1}, meanwhile recovering almost 70% of the hydrogen produced during the bioethanol steam reforming reaction with a purity higher than 99%. This would make the delivery of hydrogen for PEM fuel cells supplying – and hence the use of green bioethanol as a practical hydrogen carrier – feasible.

1. Introduction

Regarding renewable resources utilization, it is estimated that the energy potential coming from biomass in 2050 will vary in the range 50–1100 EJ/year, whereas the total global energy consumption between 600 and 1000 EJ/year [1]. Today, the bioethanol represents one of the major renewable and green sources coming from biomass (bioethanol, biodiesel, etc.), which may be produced in an anaerobic process by fermentation of sugars from plants [2]. This represents a mature method even though the cost of ethanol production is high because of the expensive feedstock plantation [3]. Otherwise, bioethanol production from lignocelluloses (the so-called 2nd bioethanol) could represent a solution to the competition between food production and bioethanol formation.

In the last two decades, a consistent literature has addressed the ethanol steam reforming (ESR) reaction in conventional fixed bed reactors for producing hydrogen [4–6] and various mechanisms were proposed, although there is not yet a general consensus about the detailed reaction pathways, due to the complexities in largely varied catalyst's constituents and reaction conditions (Table 1). ESR processes for producing hydrogen may be generally distinguished

* Corresponding author.
** Corresponding author.
E-mail addresses: a.iulianelli@itm.cnr.it (A. Iulianelli), a.basile@itm.cnr.it (A. Basile).

https://doi.org/10.1016/j.renene.2017.10.050
0960-1481/

Table 1
Possible reactions during steam reforming of ethanol.

Reaction	Equation	Comment
ESR (with sufficient steam supply)	$C_2H_5OH + 3H_2O = 2CO_2 + 6H_2$	It represents the ideal pathway, useful for the highest hydrogen production
ESR (with insufficient steam supply)	$C_2H_5OH + H_2O = 2CO_2 + 4H_2$	It represents ESR reaction without WGS reaction, indesired products and lower hydrogen production
Dehydrogenation of ethanol	$C_2H_5OH = C_2H_4O + H_2$	Reaction pathways for hydrogen production in practice
Acetaldehyde decomposition	$C_2H_4O = CH_4 + CO$	–
Acetaldehyde steam reforming	$C_2H_4O + H_2O = 3H_2 + 2CO$	–
Dehydration of ethanol	$C_2H_5OH = C_2H_4 + H_2O$	Undesired pathway with ethene formation, precursor of coke formation
Ethene decomposition	$C_2H_4 \rightarrow 2C_s + 2H_2$	Coke formation
Decomposition of ethanol	$C_2H_5OH = CO + CH_4 + H_2$	Lower production of hydrogen
Methanation	$CO + 3H_2 = CH_4 + H_2O$	Reaction of products decomposition
	$CO + 4H_2 = CH_4 + 2H_2O$	Reaction of products decomposition
Methane decomposition	$CH_4 = 2H_2 + C_s$	Reaction of products decomposition
Reaction of Boudouard	$2CO = CO_2 + C$	–
Water gas shift reaction	$CO + H_2O = CO_2 + H_2$	Reaction useful for coke formation reduction, enhancing the hydrogen production
Steam reforming of acetone	$C_3H_6O + 3H_2O = 3CO + 6H_2$	–
Steam reforming of acetic acid	$C_2H_4O_2 + 2H_2O = 2CO_2 + 4H_2$	–

into three groups: steam reforming, partial oxidation and its combination and autothermal reforming. The highest production of hydrogen can be obtained by ethanol steam reforming reaction (Eq. (1)), in which the ethanol reacts with steam to form CO_2 and hydrogen.

$$CH_3CH_2OH + 3H_2O = 2CO_2 + 6H_2 \ \Delta H_{298\ K} = 157.00\ kJ/mol \quad (1)$$

Considering the endothermic character of Eq. (1), the highest ethanol conversions are obtained at high temperatures and low pressures. However, it is well-established that the reaction pathways for ESR reaction depend on the catalyst. Therefore, ESR reaction can be expressed also as a combination of two other reversible reactions, ethanol steam reforming (insufficient steam supply) (Eq. (2)) and water-gas shift reaction (Eq. (3)):

$$C_2H_5OH + H_2O = 2CO + 4H_2 \ \Delta H_{298\ K} = 239.31\ kJ/mol \quad (2)$$

$$CO + H_2O = CO_2 + H_2 \ \Delta H_{298\ K} = -41.02\ kJ/mol \quad (3)$$

Haga et al. [6] investigated the effect of various supports in Co based catalysts for ESR reaction, indicating that a Co/Al_2O_3 shows the highest selectivity towards this reaction. Nevertheless, they observed that, when Co is supported onto SiO_2, MgO and ZrO_2, methane is produced as for the following reactions decomposition of ethanol (Eq. (4)) and methanation of CO (Eq. (5)):

$$C_2H_5OH = CH_4 + CO + H_2 \ \Delta H_{298\ K} = 33.16\ kJ/mol \quad (4)$$

$$CO + 3H_2 = CH_4 + H_2O \ \Delta H_{298\ K} = -206.2\ kJ/mol \quad (5)$$

Song et al. [3] proposed the following parallel reactions taking place during ESR:

$$C_2H_5OH = CH_3CHO + H_2 \ \Delta H_{298\ K} = 17.36\ kJ/mol \quad (6)$$

$$C_2H_5OH = C_2H_4 + H_2O \ \Delta H_{298\ K} = 28.99\ kJ/mol \quad (7)$$

$$2C_2H_5OH = (C_2H_5)2O + H_2O \ \Delta H_{298\ K} = -88.48\ kJ/mol \quad (8)$$

$$CH_4 + 2H_2O = CO_2 + 4H_2 \ \Delta H_{298\ K} = 206.2\ kJ/mol \quad (9)$$

$$2CO = CO_2 + C \ \Delta H_{298\ K} = -172.46\ kJ/mol \quad (10)$$

Therefore, the possible parallel reactions occurring during the ESR reaction in a conventional reactor seem to be the main cause of production of byproducts, besides hydrogen and CO_2, such as CO, CH_4, acetaldehyde, ethylene, ethane etc. The ESR reaction was also studied via Pd-based membrane reactor (MR) technology, because it appeared an attractive and an intensified strategy to simplify the on-site reformers due to the ability of MRs in the simultaneous generation and separation of highly concentrated hydrogen streams [5,7]. More recently, bioethanol steam reforming (BESR) reaction was studied in composite Pd-based MRs [5,8–18] and the research was aimed in decreasing the expensive Pd-content in the membranes according to the recommendation of the scientific community in the development of supported membranes [19–38]. For example, Yun et al. [8] used a composite Pd-Cu membrane, 2 μm thick, to perform the synthetic BESR in a MR, allowing for around 90% of conversion. Lin et al. [9] performed BESR reaction in a MR housing a composite Pd-Ag/Ni membrane, ~8 μm thick, over a Zn-Cu based catalyst achieving around 80% of ethanol conversion. More recently, Murmura et al. [10] obtained 4.5 mol_{H2}/mol_{EtOH} and 100% ethanol conversion at 480 °C, under 6–10 bar and over a Ni-Pt/CeO_2 catalyst, in a MR allocating a composite Pd/Al_2O_3, 4–5 μm thick, even though the presence of other byproducts in the feed was not studied. Hedayati et al. [11] firstly studied from an exergetic point of view the BESR in a composite Pd/PSS (30 μm of Pd layer) MR, loaded with a Pd-Rh/CeO_2 catalyst between 600 and 650 °C, recovering 70% of the hydrogen produced during the reaction with a yield higher than 50%. Despite these advances on BESR reaction in MRs, to the best of our knowledge no studies were done on MRs using real bioethanol mixtures coming directly from industry. Here, we present a pioneeristic study about the reforming of a real bioethanol mixture in a Pd/Al_2O_3 MR (Fig. 1), packed with a not commercial Co-Pt catalyst, obtaining a hydrogen stream with a purity >99.5 with the intent of representing a real intensified process based on membrane engineering, as also in the scopes of green chemistry [7].

2. Experimental

2.1. Materials preparation and characterization

The original substrate material used for preparing the composite membrane is porous α-Al_2O_3 (o.d., 12 mm; i. d., 8 mm; provided by GaoQ Funct. Mater. Co. (Nanjing, China). The Pd-layer deposited onto the support is around 5 μm. The whole membrane length is 7.5 cm but only 5.0 cm represents the active length. The palladium deposition was done by electroless plating at 30 °C with plating baths constituted of $PdCl_2$ (2.5 g/L), $Na_2EDTA,2H_2O$ (70 g/L) and $NH_3 \cdot H_2O$ (28%, 250 mL/L) and the reducing agent is a 0.2 moL/L hydrazine solution. Before plating, the substrate was activated with a conventional $SnCl_2/PdCl_2$ method [19]. Hence, the substrate was

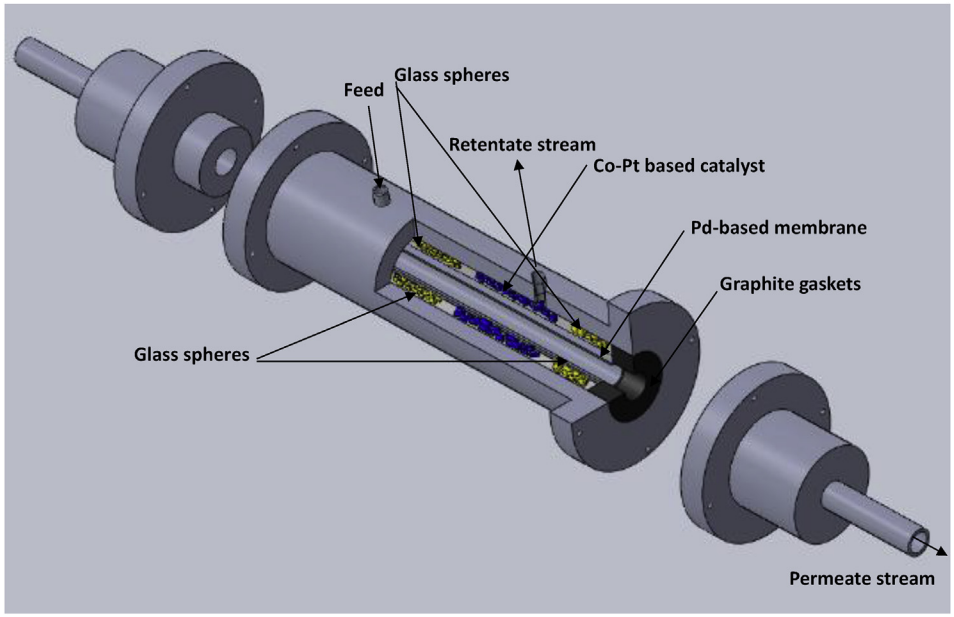

Fig. 1. Scheme of the membrane reactor used during the bioethanol steam reforming reaction with the catalyst loaded in the annulus within glass spheres.

alternately immersed in a $SnCl_2$ solution ($SnCl_2$,$2H_2O$, 5 g/L; HCl, 1 mL/L) and in a $PdCl_2$ solution ($PdCl_2$, 0.2 g/L; HCl, 1 mL/L) for around 10 min at 40 °C. Each immersion was followed by a rinse with deionized water. The aforementioned treatment was repeated for 4 times. During the typical electroless plating, a 125 mL plating bath was used for a whole plating time around 15 h. The resulting membrane was cleaned with hot water and dried overnight at 120 °C. The SEM analyses were realized by a FEI Quanta-200 instrument. The pore size distribution of the Al_2O_3 substrate was analyzed with a PSDA-20 porometer (GaoQ Funct. Mater. Co., Nanjing, China) based on the bubble-point (also known as "capillary flow") method [20]. More detailed information about the aforementioned composite Pd-based membrane preparation technology can be found in Li et al. [46]. In the post-mortem analyses, the membrane was analyzed in correspondence of the areas where defects were detected by an Auger spectroscopy (SAM), coupled with sputtering, by using a beam of argon ions with a kinetic energy of 4 kev and a current of 1 μA.

The Co(10%)Pt (3%)/CeO_2-ZrO_2-Al_2O_3 catalyst was prepared starting with the washcoat deposition on Al_2O_3 pellets (3 mm, provided by Aldrich). Mixed-oxides CeO_2-ZrO_2 (Rhodia) were dispersed in a colloidal solution for obtaining the slurry. The colloidal solution was prepared by acidifying a boehmite suspension (CeO_2-ZrO_2/AlOOH = 2/1), containing also methyl cellulose (1 wt %), with HNO_3 at pH = 4–5. Pellets were dipped in the slurry for 1 h at 80 °C and, successively, dried overnight at 120 °C, followed by calcination. The procedure was repeated until reaching a washcoat loading of about 40 wt%. Then, platinum and cobalt were deposited via wet impregnation of washcoated pellets with an aqueous solution constituted of the salt used as active metal precursor (cobalt acetate and platinum chloride, both provided by Aldrich). The impregnation procedure was carried out at 80 °C for 1 h and, then, drying overnight at 120 °C, followed by calcination at 600 °C for 3 h. Considering the bimetallic nature of the catalyst, two impregnations were performed to make the noble metal directly available at gas-solid interface. An Energy Dispersive X-ray Fluorescence (EDXRF) was used for analyzing the catalyst composition, performed using a Thermo-Scientific QUANT'X. The quantitative analysis was allowed for an Acquisition Manager software, developed through specific standard. TPR (Temperature Programmed Reduction) measurements were carried out by using a specific setup described elsewhere [47]. The stainless steel MR module was provided by ITM-CNR and shows 12 cm of whole length and 3.0 cm of o. d. It is equipped with two gaskets at both membrane ends to prevent the mixing within permeate and retentate (Fig. 1).

2.2. Experimental tests analysis

All the experimental results reported in this manuscript were obtained by analyzing the outlet streams of the MR by GC and internal standard gas procedure. Firstly, we measured the exit time of each pure gas (foreseen during the steam reforming of bioethanol) detected as a peak to the GC (Table 2). Hence, we started with the individuation of the response factors useful for the calculation of the molar flow rates of each gas coming out from the MR. For this purpose, a constant volume flow rate of nitrogen (25.0 mL/min) as internal standard gas was supplied to the MR in the whole experimental campaign. As an example, Figs. 2 and 3 show the chromatograms series (a chromatograms series consists of ten tests and, then, 10 chromatograms) containing each gas coming from retentate and permeate streams (on dry basis) during BESR reaction at 400 °C. They were useful to ensure the reproducibility of the experimental results at set operating conditions. The detection limit of all gases analyzed by GC in this work is 10 ppm. A P680 HPLC pump (Dionex) is used for supplying the bioethanol mixture, which was delivered by Green Engineering Srl. During the

Table 2
Exit time of each pure gas detected as a peak to the GC.

Pure gas	Exit time of the detected peak to the GC [min]
He	2.3
H_2	2.8
N_2	4.7
CO	5.5
CH_4	8.0
CO_2	13.5
C_2H_4	14.0

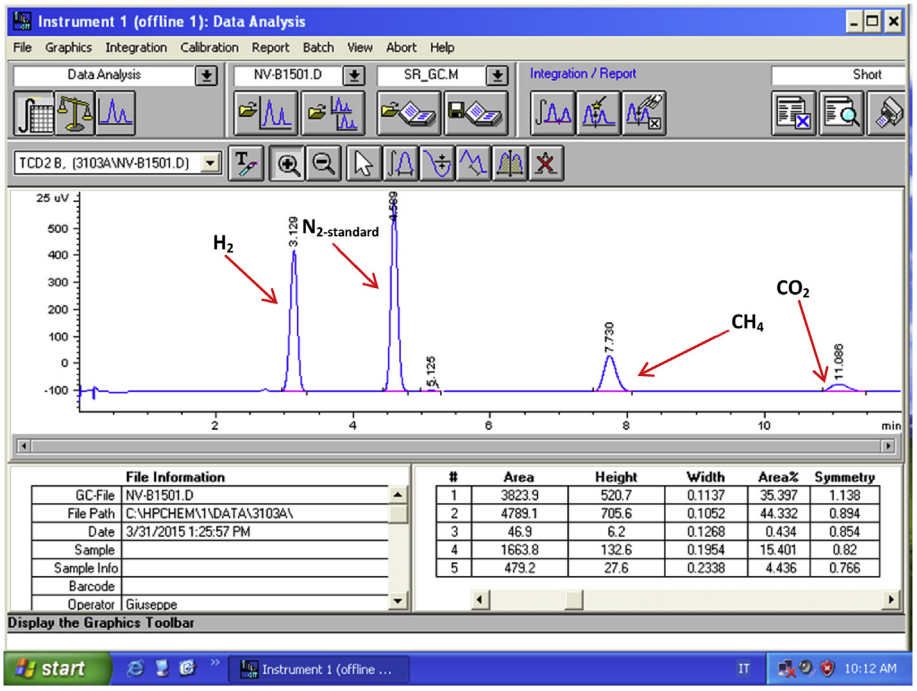

Fig. 2. Chromatogram (test n. 3) for the retentate stream (dry basis) during BESR reaction in the composite Pd/Al_2O_3 MR at T = 400 °C, p = 2.0 bar, GHSV = 1900 h^{-1}.

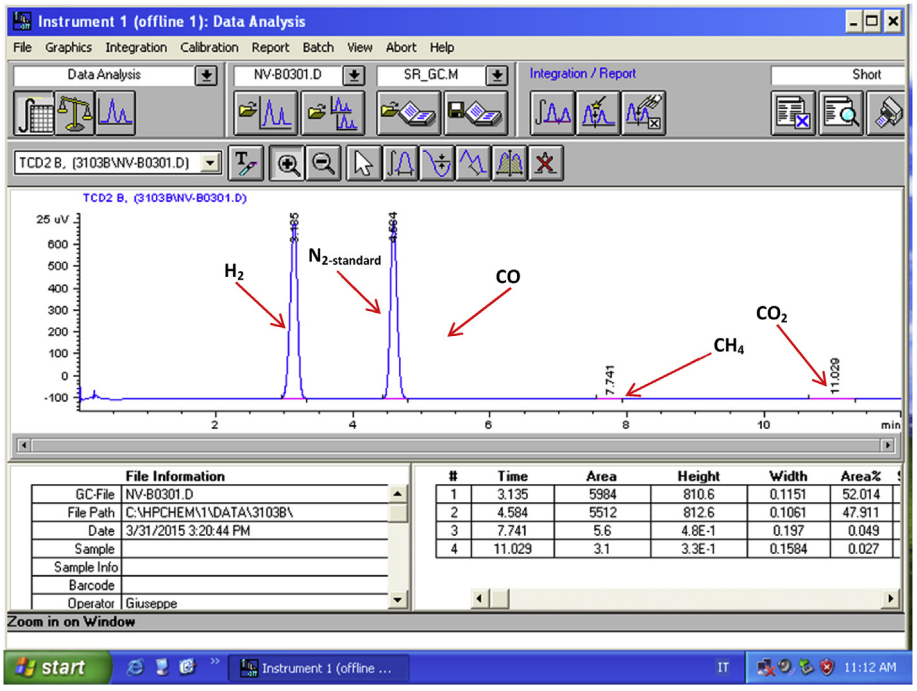

Fig. 3. Chromatogram (test n. 3) for the permeate stream (dry basis) during BESR reaction in the composite Pd/Al_2O_3 MR at T = 400 °C, p = 2.0 bar, GHSV = 1900 h^{-1}.

industrial production of the aforementioned bioethanol, the concentration of the various compounds can vary as represented in Table 3. The H_2O/EtOH feed molar ratio is equal to 6/1. Afterwards, the total liquid feed mixture is vaporized and mixed with a constant flow rate of nitrogen (25.0 mL/min), as internal standard gas, and flowed into the annulus of the MR, in which a Co(10%)Pt (3%)/CeO_2-ZrO_2-Al_2O_3 catalyst is loaded. Prior to be inserted in the MR, the catalyst was reduced by using hydrogen and helium at 400 °C for 2 h. Hence, the experimental tests about the BESR reaction are carried out at a gas hourly space velocity (GHSV) ranging from 1900 to 4800 h^{-1}. Before the experimental tests, the MR module is checked for leakages by flowing helium in the annulus at 25 °C. Then, the MR is heated up till 400 °C using a heating tape connected to a temperature controller, measuring the operating temperature by a thermocouple inserted into the annulus of the MR. The reaction pressure is regulated by means of a back-pressure controller

Table 3
Real bio-ethanol mixture composition and test method.

Property	Unit	Limits		Test Method
		Minimum	Maximum	
Ethanol content + higher saturated alcohols	% (m/m)	98,7		EC/2870/2000 - method I, Appendix II, Method B
Higher saturated (C3 - C5) mono-alcohols content	% (m/m)		2,0	EC/2870/2000 - method III
Methanol content	% (m/m)		1,0	EC/2870/2000 - method III
Water content	% (m/m)		0,3	EN 15489
Inorganic chloride content	mg/L		20,0	EN 15489 or prEN 15492
Copper content	mg/kg		0,1	EN 15488
Total acidity (expressed as acetic acid)	% (m/m)		0,007	EN 15491
Appearance	–		Clear and bright	Visual inspection
Phosphorous content	mg/L		0,5	EN 15487
Non-volatile material content	mg/100 mL		10	EC/2870/2000 - method II
Sulphur content	mg/kg		10	EN 15485 or EN 15486

placed at the outlet side of the retentate stream and ranges between 1.5 and 2.0 bar, while during the whole experimental campaign the permeate pressure is kept constant at 1.0 bar. A sweep gas (N_2) flow rate of 25.0 mL/min is supplied in the permeate side in counter-current modality with respect to the feed flow by a mass-flow controller (Brooks Instruments 5850 S) driven by a computer software provided by Lira (Italy). Under BESR operation, the retentate stream goes through a cold trap for removing the vapor fraction; then, the permeate and the retentate gaseous streams are analyzed simultaneously in a temperature programmed HP 6890 gas chromatograph (GC) with a thermal conductivity detector (TCD) at 250 °C and He as carrier gas. The GC is equipped by three packed columns: Porapack R 50/80 (8 ft × 18 in) and Carboxen 1000 (15 ft × 18 in) connected in series. This apparatus is driven by a software provided by Hewlett-Packard. About the reaction tests, each experimental point reported in this work is determined by GC analysis (15 min each one) via internal standard gas procedure and represents an average value of, at least, ten experimental points (reaction cycle), taken in 150 min of GC analyses at steady-state conditions.

For each experimental point reported in this work, the carbon balance closure has been checked for ensuring the validity of the experimental results.

2.3. Permeation tests through the Pd/Al_2O_3 membrane

The hydrogen perm-selectivity characteristics of the supported Pd/Al_2O_3 membrane are evaluated by pure gas permeation tests (N_2, H_2, CH_4, He), at 400 °C and transmembrane pressures (Δp) equal to 0.5 and 1.0 bar, in conditions of fresh membrane and after each reaction cycle for ensuring the performance stability as well. The volume flow rate of each pure gas permeating through the membrane is measured by means of a bubble-flow meter as an average value of, at least, 10 experimental points. The ideal selectivity of hydrogen with respect to the other gases is expressed as indicated in Eq. (11):

$$\alpha_{H2/i} = J_{H2}/J_i \; (i = N_2, He, CH_4) \tag{11}$$

Where, J_{H2} and Ji are the hydrogen permeating flux and the permeating flux of another reference gas among He, N_2 and CH_4.

3. Results and discussion

3.1. Composite Pd/Al_2O_3 membrane characterization

The cross section of the Pd/Al_2O_3 composite membrane was analyzed by SEM microscopy and the image reported in Fig. 4(a) shows the cross-sectional view, illustrating clearly the palladium layer (in white colour) deposited onto the Al_2O_3 substrate. The latter has a typical asymmetric structure, subdivided in a microporous surface layer, an intermediate layer and a macroporous base. Fig. 4(b) shows the characteristic cauliflower morphology of the palladium layer, which presented a strong adhesion to the support with a uniform thickness of approximately 5.0 μm. Fig. 4(c) shows that the composite membrane before experimental tests is highly lustrous, without any blistering or peeling. The palladium layer is smooth and significant defects are absent. The uniformity of the Pd-layer thickness was verified according to the volume of the plating bath, indicating that our plating process can sufficiently transfer palladium ions to the membrane support. The permeation of hydrogen through the palladium follows a solution-diffusion mechanism [29] and the law is represented by the general expression reported in Eq. (12):

$$J_{H2} = Pe \cdot (p^n_{H2\text{-retentate}} - p^n_{H2\text{-permeate}}) \; [mol/m^2 \cdot s] \tag{12}$$

where, Pe is the hydrogen permeance, $p_{H2\text{-retentate}}$ and $p_{H2\text{-permeate}}$ the hydrogen partial pressures in the retentate and permeate sides, respectively, and n (variable in the range 0.5–1) the dependence factor of the hydrogen flux on the hydrogen partial pressure. Before the BESR reaction tests, the hydrogen perm-selectivity characteristics of the composite membrane were investigated under pure gas permeation tests at 400 °C and 0.5 and 1.0 bar of transmembrane pressures. The analyses demonstrated that only hydrogen permeates through the membrane at onset condition, ensuring a full hydrogen perm-selectivity with respect to the other gases (Table 4). As a consequence, the coefficient “n” of Eq. (13) is equal to 0.5, useful value for indicating Sieverts-Fick law (Eq. (13)), regulating the permeation of hydrogen through hydrogen fully perm-selective membranes.

$$J_{H2} = Pe \cdot (p^{0.5}_{H2\text{-retentate}} - p^{0.5}_{H2\text{-permeate}}) \; [mol/m^2 \cdot s] \tag{13}$$

The graphical assessment of the coefficient “n”, as a function of the linear regression index (R^2), confirmed the validity of Sieverts-Fick law, being the R^2 index, at n = 0.5, the highest one (Fig. 5). Furthermore, starting from the preliminary experimental results on the Pd/Al_2O_3 membrane of this work, we compared its characteristics to other composite membranes studied in the specialized literature [21–38], demonstrating its high potentiality over the other ones (Table 5). The Pd/Al_2O_3 membrane confirmed high performance at 400 °C and 0.5 bar of transmembrane pressure, showing a great hydrogen permeance ($4.3 \cdot 10^{-4}$ moL/m^2 s Pa), considering the lower temperature and transmembrane pressure adopted in this work compared to the results of Sanz et al. [24] ($4.5 \cdot 10^{-4}$ moL/m^2 s Pa), Rothenberger et al. [27] ($2.7 \cdot 10^{-4}$ moL/m^2 s Pa) and Wang et al. [32] ($1.7 \cdot 10^{-4}$ moL/m^2 s Pa). This result is

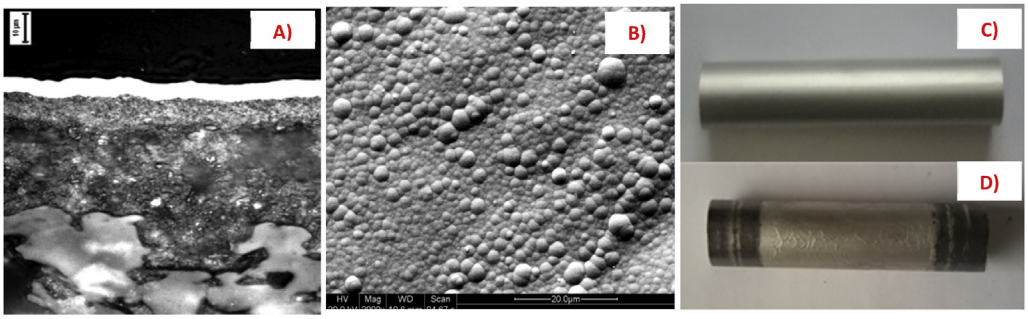

Fig. 4. Metallographic image of the cross section of the composite Pd/Al_2O_3 membrane (a); SEM image of the palladium surface morphology (b); the composite membrane at onset of experimental tests (c); the composite membrane at the end of the experimental campaign (d).

Table 4
Ideal selectivity and permeating flux of pure gases through the Pd/Al_2O_3 composite membrane at different transmembrane pressure, and at 400 °C (onset conditions) and 450 °C (after 500 h under operation).

T [°C]	Δp [bar]	J_{H2} [mol/m^{2}s]	J_{N2} [mol/m^{2}s]	J_{CH4} [mol/m^{2}s]	J_{He} [mol/m^{2}s]	$\alpha_{H2/N2}$	$\alpha_{H2/CH4}$	$\alpha_{H2/He}$
400	0.5	21.7	N.D.	N.D.	N.D.	∞	∞	∞
	1.0	36.8	N.D.	N.D.	N.D.	∞	∞	∞
450	0.5	38.3	$1.8\cdot10^{-2}$	$3.2\cdot10^{-2}$	$3.5\cdot10^{-2}$	2100	1200	1100
	1.0	67.1	$4.5\cdot10^{-2}$	$6.3\cdot10^{-2}$	$8.4\cdot10^{-2}$	1500	1070	800

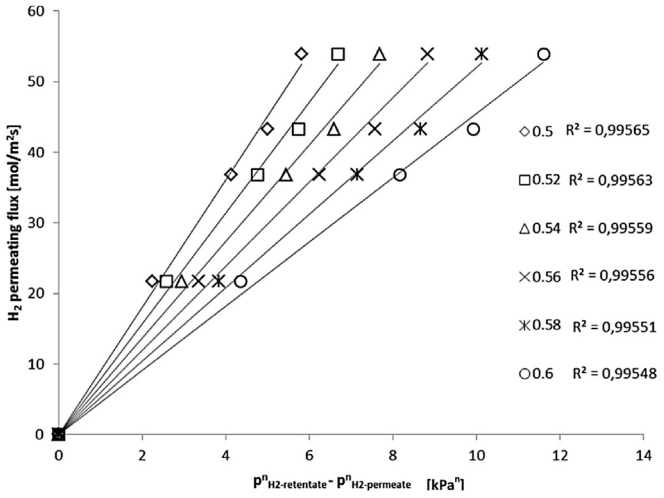

Fig. 5. Graphical assessment of coefficient "n" as a function of linear regression index (R^2) for the hydrogen permeating flux through the composite Pd/Al_2O_3 membrane vs transmembrane pressure at different "n".

also relevant in terms of palladium-saving because our composite membrane was constituted of a thinner Pd-layer (5 μm) than the aforementioned membranes (a part from Wang et al. [32], with the same Pd-layer). Much thinner membranes are also reported in Table 5, but they did not show full hydrogen perm-selectivity.

3.2. Co-Pt/CeO_2-ZrO_2-Al_2O_3 catalyst

Before using the Co-Pt catalyst in BESR reaction, its composition was determined via XRF analysis, obtaining 3.3% of Pt, 10.5% of Co, 14.5% of CeO_2, 10.9% ZrO_2 and 60.8% Al_2O_3. TPR measurements (Fig. 6), done on some samples, showed a lower temperature peak at 197 °C, ascribable to PtO_2 reduction [39], whereas the cobalt oxide reduction peak was observed at 429 °C, higher than the typical reduction temperatures reported in literature for this species [40]. Furthermore, we observed that the cobalt oxide reduction involves a Co_3O_4 reduction to CoO and, then, to Co. This was probably caused by the presence of Al_2O_3 in the CeO_2-ZrO_2 slurry, which inhibited the reduction of CoO, because Al_2O_3 may establish a solid solution with CoO, difficult to be reduced [41]. The peak recorded at 550 °C may be linked to the superficial reduction of CeO_2-ZrO_2. A Microcal Origin software made us able to deconvolute the reduction curve after background subtraction via least-squares fitting to Gaussian–Lorentzian functions. Observing the profile of the deconvolution, it was possible to estimate the hydrogen uptake during the reduction, compared to theoretical values, calculated according to the metals loadings (Table 6). The experimental H_2-uptake of the PtO_2 reduction resulted higher than the theoretical value, whereas it was lower for the complete Co_3O_4 reduction to Co. This may be explained with the reduction of Co_3O_4 at lower temperatures; meanwhile, the Pt supported on the CeO_2-ZrO_2 may reduce early the adjacent Co particles to CoO owing to the hydrogen activation through a spillover mechanism [42]. The further reduction of CoO to Co was observed only at higher temperatures because of the solid solution formation.

3.3. BESR reaction tests

The BESR reaction tests were carried out at 400 °C, by varying the GHSV from 1900 to 4800 h^{-1} and the reaction pressure from 1.5 to 2.0 bar. For each experimental cycle, the carbon balance closure between in and out of the MR was checked and the maximum error was not higher than 2%. Although the ethanol conversion is unfavored from a thermodynamic point of view by an increase of pressure (ethanol steam reforming reaction proceeds towards the products with an increase of moles number), at GHSV = 1900 h^{-1} the ethanol conversion increased from 50% at 1.5 bar to ~ 60% at 2.0 bar (Fig. 7). This was due to the equilibrium shift promoted by a higher hydrogen permeation driving force (see Eq. (13)), consequent to a pressure increase. This allowed a larger removal of hydrogen from the reaction to the permeate side, shifting the reaction towards the products (Le Chatelier principle). By increasing the GHSV, being shorter the contact time within the reactants and

Table 5
Characteristics and performance of the composite Pd/Al_2O_3 membrane of this work compared to other representative and recent literature data.

Membrane type	Preparation method	Pd layer (μm)	T (°C)	Δp (Pa)	H_2 permeance (mol/m^2·s·Pa)	Ideal Selectivity ($\alpha_{H2/N2}$)	Reference
Pd/(γ-Al_2O_3/Al_2O_3)	ELP	5	500	400000	$2.8\cdot10^{-6}$	8000	[21]
Pd/(γ-Al_2O_3/Al_2O_3)	ELP	2.4	500	100000	$3.9\cdot10^{-6}$	32500	[22]
Pd/PSS	ELP	10	400	200000	$8.7\cdot10^{-7}$	~11800	[23]
Pd/YSZ/PSS	ELP	28	450	40000	$4.5\cdot10^{-4}$[a]	∞	[24]
Pd/(γ-Al_2O_3/Al_2O_3)	ELP	2.6	370	400000	$4.8\cdot10^{-7}$	3000	[25]
Pd/Al_2O_3	CVD	2	300	30000	$3.3\cdot10^{-6}$	5000	[26]
Pd/Fe_2O_3/PSS	ELP	22	450	100000	$2.7\cdot10^{-4}$[a]	∞	[27]
Pd/(γ-Al_2O_3/Al_2O_3)	ELP	6	480	100000	$2.6\cdot10^{-6}$	2100	[28]
Pd/Al_2O_3	ELP	0.9	460	199000	$3.1\cdot10^{-6}$	1200	[29]
Pd/PSS	ELP	10	400	200000	$5.0\cdot10^{-7}$	5000	[30]
Pd/Al_2O_3	ELP	0.9	450	105000	$4.0\cdot10^{-6}$	9200	[31]
Pd-Ag-Ru/α-Al_2O_3	ELP	6	500	100000	$1.7\cdot10^{-4}$[a]	∞	[32]
Pd–Cu/SiO_2/Ni–SS	VED	<2	460	70000	–	>80000	[33]
Pd-Ag/SS	Sputtering	2.6	450	1000000	$3.0\cdot10^{-6}$	500[b]	[34]
Ru/Pd/Al_2O_3/PHA	ELP	6.8	500	100000	–	∞ (H_2/He)	[35]
Pd/PSS	PP-ELP	20	450	–	–	∞	[36]
Pd/YSZ/PSS	ELP	25–30	500	–	$3.1\cdot10^{-4}$[a,c]	400[b]	[37]
Pd/Al_2O_3	ELP	2–4	400	–	–	500	[38]
Pd/Al_2O_3	ELP	5	400	100000	$4.3\cdot10^{-4}$	∞	**This work**

[a] Sieverts-Fick law considered.
[b] Value obtained as separation factor using H_2/N_2 mixture.
[c] [mol/^{m2}·s·$Pa^{0.5}$].

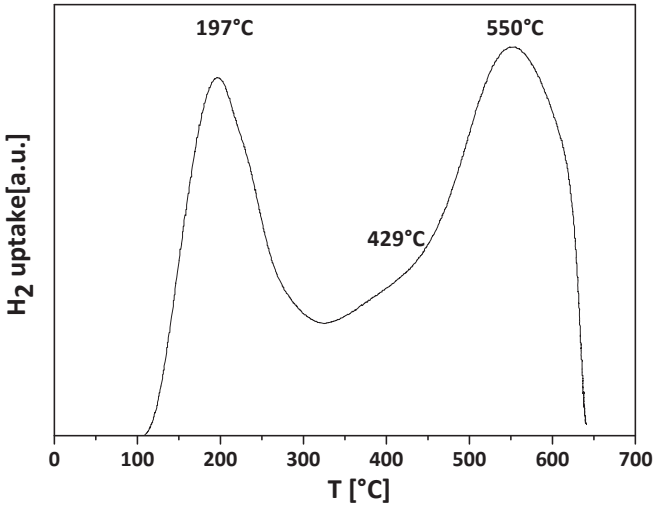

Fig. 6. TPR profile of Pt-Co/CeO_2-ZrO_2-Al_2O_3 catalyst.

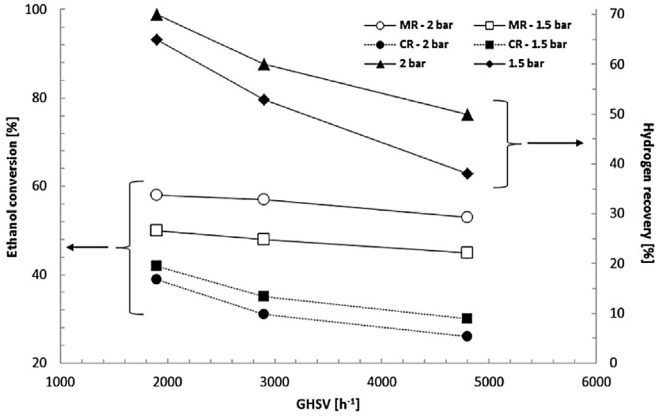

Fig. 7. Ethanol conversion (for MR and CR) and hydrogen recovery vs space velocity (GHSV) during BESR reaction over Co-Pt based catalyst in the composite Pd/Al_2O_3 membrane reactor at T = 400 °C, H_2O/EtOH = 6/1 and different reaction pressure.

the catalyst, the conversion decreased at both the reaction pressures investigated. Fig. 7 also shows how the conversions in the MR are always higher than the equivalent CR in the whole experimental conditions used in this work. This is due to the shift effect present in the MR, which is responsible of an enhancement of the ethanol conversion. On the contrary, in the equivalent CR, the higher the pressure the lower the conversion because of the thermodynamic effect. The recovery of hydrogen was promoted by an increase of reaction pressure because, according to Sieverts-Fick law, a more consistent removal of hydrogen from the reaction side was allowed, globally favouring an increase of hydrogen collected in the permeate side.

On the contrary, at higher GHSV value, the conversion of hydrogen was reduced with a consequent depletion of hydrogen production. As a result, the hydrogen permeation driving force was depressed and the recovery decreased. At 2.0 bar and GHSV = 1900 h^{-1}, the maximum hydrogen recovered over the total produced during BESR reaction was 70%. It is worth of noting that the main goal of this work was the purity of hydrogen reached in the permeate stream. Indeed, at the operating conditions used in this work, the average value of the hydrogen purity was never lower than 99% (Fig. 8, sketching the hydrogen permeate purity at 400 °C and 1.5 bar of reaction pressure at different GHSV values). As shown, the maximum hydrogen purity in the permeate stream was 99.7%, reached at 400 °C, 2.0 bar and GHSV = 4800 h^{-1}. After each

Table 6
Experimental and theoretical hydrogen up-take for active reduction species.

Active reduction species	T [°C]	Experimental H_2-uptake [mmol/g_{CAT}]	Theoretical H_2-uptake [mmol/g_{CAT}]
Pt (PtO_2 → Pt^0)	197	937	307
Co (Co_3O_4 → Co^0)	429	1690	2262

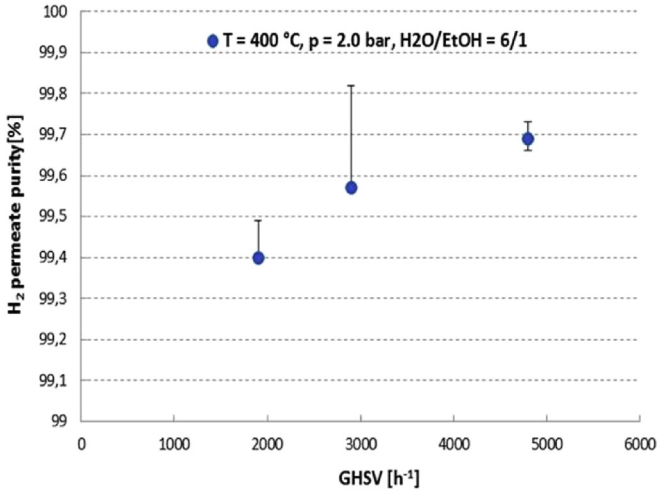

Fig. 8. Hydrogen permeate purity vs space velocity (GHSV) during BESR reaction over Co-Pt based catalyst in a composite Pd/Al_2O_3 membrane reactor at 400 °C and 2.0 bar of reaction pressure.

reaction test, pure hydrogen was flowed into the reaction side (~$3.0 \cdot 10^{-3}$ moL/min) at 400 °C and for around 2 h in order to detect methane formation to the GC, as a confirmation of coke formation (no oxygen can be used for avoiding the oxidation of the metallic layer of the composite membrane). In all cases, no methane was detected to the GC and, then, coke formation was excluded. In the meanwhile, in order to evaluate the membrane exposure to sulphur/phosphorous compounds present in the feed, after each reaction cycle, the hydrogen permeating flux through the membrane was checked and compared to the value obtained initially, with the membrane in fresh condition. Then, by expressing the stability of the membrane in terms of H_2/N_2 ideal selectivity over the operating time, during 500 h with the membrane under operation and after several reaction cycles, further pure gas permeation tests evidenced the permeation of solely hydrogen through the membrane, confirming its full hydrogen perm-selectivity, not affected negatively by the exposure to sulphur/phosphorous compounds. Hence, the experimental results obtained in this work were compared to other recent studies in literature dealing with steam reforming of bio-ethanol in MRs [8–11,14–18,43–45]. This comparison is only qualitative, because, a part from this work, all the results reported in Table 7 were obtained by supplying synthetic bioethanol mixtures not containing sulphur and phosphorous in the feed. Hence, their poisoning effects on the membranes and the catalysts housed in the considered MRs were not evaluated. Among the latest advancements on BESR reaction in MRs housing composite membranes, the present work showed – in our opinion – great performance in terms of recovery (70%) and purity of hydrogen (>99.5%, without any traces of CO), making the permeate stream useful for low temperature PEM fuel cells supplying. Particular emphasis should be also given to the low Pd-content shown by the composite membrane of this study, only comparable to the membranes of Yun et al. [8], Lin et al. [9] and Murmura et al. [10]. In the same table, we reported also some literature data about dense self-supported Pd-based membranes allocated in MRs. Considering the membrane thickness, it is evident that the amount of palladium is quite high, making these membranes not a competitive solution for the scaling-up of BESR process in MRs at industrial level. Nevertheless, even considering the maximum conversion of ethanol obtained in this work (60% at 2 bar and GHSV = 1900 h^{-1}), compared to all of the other significative literature data of Table 7, it resulted consistently lower. As stated above, excluding the negative effect given by the sulphur and phosphorous in the feed on the membrane, the reason why the ethanol conversion of this work was depressed has to be found in their effect on the Co-Pt catalyst. Indeed, as demonstrated in the specialized literature [12,13], the presence of sulphur could be responsible of a lower catalytic activity of the bimetallic catalyst and, consequently, of the decrease of ethanol conversion. This was indirectly demonstrated because, although out of the scopes of this work, before loading the Co-Pt based catalyst in the MR, it was tested in a conventional reactor by performing the ESR reaction at atmospheric pressure between 300 and 600 °C and GHSV = 4800 h^{-1}, using a pure H_2O/EtOH mixture with feed ratio 3/1 (Fig. 9). Total ethanol conversion was recorded in the low-temperature range and a fairly good agreement with thermodynamic predictions was observed at T > 450 °C. These results demonstrate that, without the presence of sulphur and phosphorous in the feed (instead of the real bio-ethanol mixture of this work), the catalytic activity of Co-Pt catalyst allowed complete conversion in the whole range of temperatures investigated. Consequently, for improving the conversion in the MR, the reaction temperature was increased up to 450 °C and new pure gas permeation tests were performed in terms of permeating flux and ideal selectivity at both 0.5 and 1.0 bar of transmembrane pressure (Table 4).

The observed finite values of the ideal selectivity of hydrogen over other reference gases demonstrated that the increase of reaction temperature induced some defects on the membrane surface. Indeed, the loss of the full hydrogen perm-selectivity of the composite membrane at 450 °C was probably due to the formation

Table 7
Membrane characteristics, performances and operating conditions during BESR reaction in MRs: this work compared to published data in the specialized literature.

Membrane housed in the MR	Dense metallic layer [μm]	H_2O/C_2H_5OH	T [°C]	p [bar]	Conversion [%]	H_2 recovery [%]	H_2 yield [%]	H2 purity [%]	Reference
composite Pd/Al_2O_3	5	6/1	400	2.0	60	70	35	~99.6	**This work**
composite Pd-Cu	2	13/1	360	1.0	74	–	–	–	Yun et al. [8]
composite Ni-Pd-Ag	<8	3/1	450	3.0	~80	–	70	>90	Lin et al. [9]
composite Pd/Al_2O_3	4–5	–	480	10	90	–	80	>99	Murmura et al. [10]
composite Pd-Ag/PSS	30	–	650	4.0	100	70	>50	–	Hedayati et al. [11]
composite Pd-Ag/PSS	30	3/1	600	16	–	80	85	–	Espinal et al. [14]
composite Pd-Ag	30	12/1	700	6.9	–	–	75	–	Papadias et al. [15]
composite Pd on PSS	25	3/1	400	8.0	100	55	–	~95	Basile et al. [16]
composite Pd on PSS	25	13/1	400	12.0	87	12	17	~95	Seelam et al. [17]
self-supported Pd-Ag	75	10/1	550	–	~100	80	<50	≈100	da Silva et al. [18]
self-supported Pd-Ag	50	18.7/1	400	3.0	~100	90	53	≈100	Iulianelli et al. [43]
self-supported Pd-Ru	50	–	450	1.0	–	–	~50	≈100	Mironova et al. [44]
self-supported Pd-Ag	150	10/1	450	5.0	–	93[b]	70[a]	≈100	Borgognoni et al. [45]

[a] H2 yield **COx-free** = H2 permeate/6·EtOHfeed
[b] Calculated.

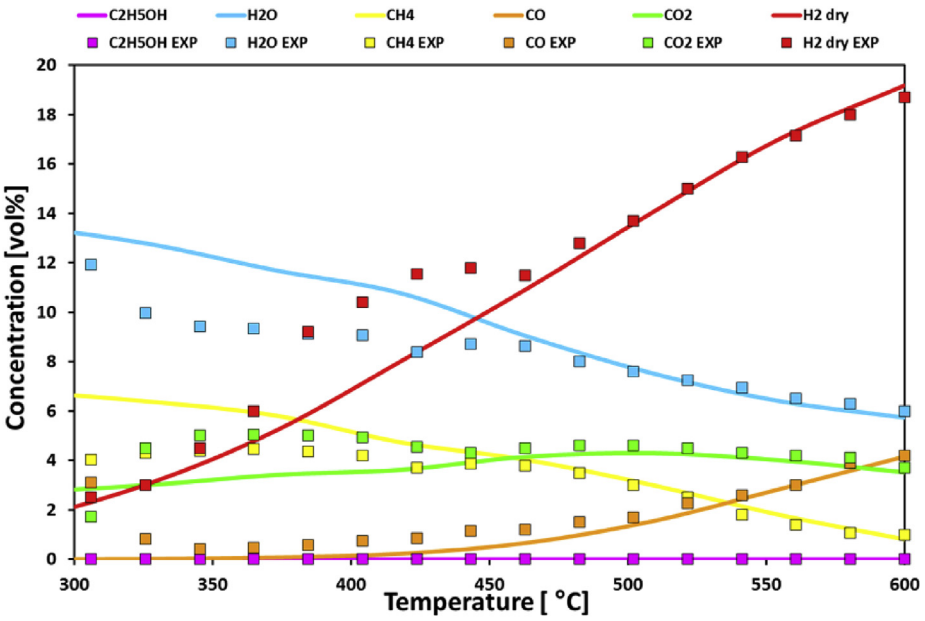

Fig. 9. Products gas distribution as a function of reaction temperature during ESR reaction in a conventional reactor under a pure H_2O/C_2H_5OH (feed ratio = 3/1) mixture, GHSV = 4800 h^{-1}, p = 1 bar.

of pin-holes, responsible of the permeation of other gases beside hydrogen (Table 4). Therefore, the MR was cooled down at room temperature for analyzing the status of the membrane and the possible damages produced by the temperature increase above 400 °C.

Then, we observed the presence of damages (wrinkles) on the membrane surface (Fig. 2(d)), probably caused by the temperature increase above 400 °C, responsible of the thermal expansion of the materials constituting the composite membrane. In fact, the palladium layer dilatation in the axial direction was not allowed owing to the presence of gaskets blocking the membrane to the MR module at both ends, making the wrinkles formation possible, with consequent formation of micro-cracks and small pin-holes in the Pd-layer (Fig. 10). In the post mortem analyses, SAM tests on the membrane surfaces were carried out at three different locations (particularly where the presence of defects was observed), evidencing absence of carbon, phosphorous and sulphur contamination, while a very low concentration of chloride was detected, probably as a residual of $PdCl_2$, used in the electroless bath for the Pd-deposition, probably not completely removed by the subsequent rinsing.

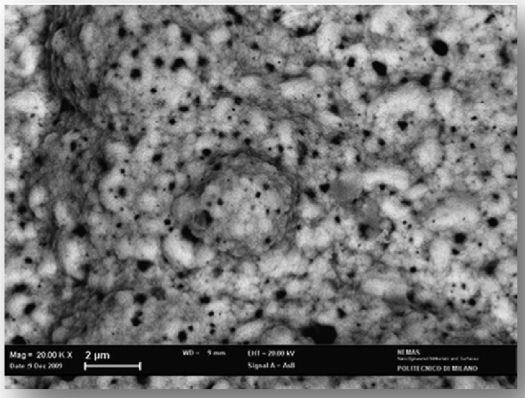

Fig. 10. Presence of pin-holes in the Pd-layer at the end of the experimental tests.

4. Conclusions

To the best of our knowledge, most of the research developed about the steam reforming of bio-ethanol refers to the utilization of synthetic bioethanol mixture (or, more easily, ethanol/water mixtures) in fixed bed reactors, paying more attention to the role of the catalyst towards conversion and product selectivity, but no one investigated the reforming of a real bioethanol mixture coming from industry in a MR, developing an intensified process producing as much as possible pure hydrogen. Then, it was used in a steam reforming process for producing hydrogen in a supported thin Pd-membrane reactor, recovering at 400 °C and 2.0 bar 70% of hydrogen, with the least purity of ~99.5%, without being affected by the exposure to sulphur, phosphorous and coke deposition. Furthermore, this work demonstrates feasible the combination of the bioethanol exploitation, as a renewable and green hydrogen carrier, and the advantages of the MR utilization for producing highly concentrated hydrogen in an intensified process. As a next challenge, the Co-Pt based catalyst used in this work will be further studied to analyse in deep the negative effects due to the sulphur and/or phosphorous exposure on the catalytic activity. Furthermore, further research will be necessary for making possible higher ethanol conversions, also at temperatures lower than 400 °C. Meanwhile, based on the results of this work, another critical issue needing solution will be constituted by the negative effect on the composite Pd-based membranes used in this work of an operating temperature above 400 °C. The next study will focus on a technological evolution of the proposed membranes, which will be closed at one end to facilitate the elongation during the heating up procedure for avoiding the formation of pin-holes caused by the temperature increase. Last but not least, a life cycle assessment of bioethanol and a full analysis of the whole process proposed here will constitute an advancement of this work.

Acknowledgements

The Authors are grateful to Green Engineering Srl for providing the real bio-ethanol mixture used in this work.

References

[1] G. Fischer, L. Schrattenholzer, Biomass Bioen. 20 (2001) 151.
[2] R. Trane, S. Dahl, M.S. Skjøth Rasmussen, A.D. Jensen, Int. J. Hydrogen En. 37 (2012) 6447.
[3] J. Llorca, V.C. Corberán, N.J. Divins, R.O. Fraile, E. Taboada, Hydrogen from bioethanol, Ch. 7, in: L.M. Gandia, G. Arzamendi, P.M. Dieguez (Eds.), Renewable Hydrogen Technologies, Elsevier, 2013, pp. 1–472. ISBN: 978-0-444-56352-1.
[4] H. Song, L. Zhang, R.B. Watson, D. Braden, U.S. Ozkan, Catal. Today 129 (2007) 346.
[5] A. Iulianelli, A. Basile, Catal. Sci. Techn. 1 (2011) 366.
[6] F. Haga, T. Nakajima, K. Yamashita, S. Mishima, React. Kinet. Catal. Lett. 63 (1998) 253.
[7] E. Drioli, A. Brunetti, G. Di Profio, G. Barbieri, Green Chem. 14 (2012) 1561.
[8] S. Yun, H. Lim, S.T. Oyama, J. Membr. Sci. 409–410 (2012) 222.
[9] W.-H. Lin, Y.-C. Liu, H.-F. Chang, Int. J. Hydrogen En. 35 (2010) 12961.
[10] M.A. Murmura, M. Patrascu, M.C. Annesini, V. Palma, C. Ruocco, M. Sheintuch, Int. J. Hydrogen En. 40 (2015) 5837.
[11] A. Hedayati, O. Le Corre, B. Lacarrière, J. Llorca, Int. J. Hydrogen En. 40 (2015) 3574.
[12] A. Iulianelli, S. Liguori, Y. Huang, A. Basile, J. Power Sou. 273 (2015) 25.
[13] C.G. Visconti, L. Lietti, P. Forzatti, R. Zennaro, Appl. Catal. A Gen. 330 (2007) 49.
[14] R. Espinal, A. Anzola, E. Adrover, M. Roig, R. Chimentao, F. Medina, E. Lopez, D. Borio, J. Llorca, Int. J. Hydrogen En. 39 (2014) 10902.
[15] D.D. Papadias, S.H.D. Lee, M. Ferrandon, S. Ahmed, Int. J. Hydrogen En. 35 (2010) 2004.
[16] A. Basile, P. Pinacci, A. Iulianelli, M. Broglia, F. Drago, S. Liguori, T. Longo, V. Calabrò, Int. J. Hydrogen En. 36 (2011) 2029.
[17] P.K. Seelam, S. Liguori, A. Iulianelli, P. Pinacci, F. Drago, V. Calabrò, M. Huuhtanen, R. Keiski, V. Piemonte, S. Tosti, M. De Falco, A. Basile, Catal. Today 193 (2012) 42.
[18] A.M. da Silva, L.V. Mattos, J. Múnera, E. Lombardo, F.B. Noronha, L. Cornaglia, Int. J. Hydrogen En. 40 (2015) 4154.
[19] S. Shu, Y. Huang, X. Hu, Y. Fan, N. Xu, J. Phys. Chem. C 113 (2009) 19618.
[20] J. Yu, X. Hu, Y. Huang, Sep. Purif. Tech. 70 (2010) 314.
[21] D.A.P. Tanaka, M.A.L.T. Nagase, J. Okazaki, Y. Wakui, F. Mizukami, T.M. Suzuki, Adv. Mater 18 (2006) 630.
[22] H. Li, A. Goldbach, W. Li, H. Xu, J. Membr. Sci. 299 (2007) 130.
[23] C. Mateos-Pedrero, H. Silva, D.A. Pacheco Tanaka, S. Liguori, A. Iulianelli, A. Basile, A. Mendes, Appl. Catal. B Env. 174 (2015) 67.
[24] R. Sanz, J.A. Calles, D. Alique, L. Furones, S. Ordóñez, P. Marín, P. Corengia, E. Fernandez, Int. J. Hydrogen En. 36 (2011) 15783.
[25] B.K.R. Nair, J. Choi, M.P. Harold, J. Membr. Sci. 288 (2007) 67.
[26] N. Itoh, T. Akiha, T. Sato, Catal. Today 104 (2005) 231.
[27] K.S. Rothenberger, A.V. Cugini, B.H. Howard, R.P. Killmeyer, M.V. Ciocco, B.D. Morreale, R.M. Enick, F. Bustamante, I.P. Mardilovich, Y.H. Ma, J. Membr. Sci. 244 (2004) 55.
[28] X. Zhang, G. Xiong, W. Yang, J. Membr. Sci. 314 (2008) 67.
[29] S. Yun, S.T. Oyama, J. Membr. Sci. 375 (2011) 28.
[30] P.P. Mardilovich, Y. She, Y.H. Ma, M.H. Rey, AIChE J. 44 (1998) 310.
[31] T. Maneerung, K. Hidajat, S. Kawi, J. Membr. Sci. 452 (2014) 127.
[32] L. Wang, R. Yoshiie, S. Uemiya, J. Membr. Sci. 306 (2007) 1.
[33] S.E. Nam, K.H. Lee, J. Membr. Sci. 192 (2001) 177.
[34] T.A. Peters, W.M. Tucho, A. Ramachandran, M. Stange, J.C. Walmsley, R. Holmestad, A. Borg, R. Bredesen, J. Membr. Sci. 326 (2009) 572.
[35] S.K. Ryi, A. Li, C.J. Lim, J.R. Grace, Int. J. Hydrogen En. 36 (2011) 9335.
[36] R. Sanz, J.A. Calles, S. Ordóñez, P. Marín, D. Alique, L. Furones, J. Membr. Sci. 446 (2013) 410.
[37] G. Straczewski, J. Völler-Blumenroth, H. Beyer, P. Pfeifer, M. Steffen, I. Felden, A. Heinzel, M. Wessling, R. Dittmeyer, Chem. Eng. Proc. 81 (2014) 13.
[38] A. Goldbach, F. Bao, C. Qi, C. Bao, L. Zhao, C. Hao, C. Jiang, H. Xu, Int. J. Greenh. Gas. Contr. 33 (2015) 69.
[39] R.J. Woo, D. Moon, L.D. Sang, D. Lee, S. Hong, Theor. Appl. Chem. Eng. 10 (2004) 1024.
[40] R. Padilla, M. Benito, L. Rodrìguez, A. Serrano, G. Munoz, L. Daza, Int. J. Hydrogen En. 35 (2010) 8921.
[41] Z. Lendzion-Bieluń, R. Jędrzejewski, W. Arabczyk, Cent. Eur. J. Chem. 9 (2011) 834.
[42] A. Norman, V. Perrichon, A. Bensaddik, S. Lemaux, H. Bitter, D. Koningsberger, Top. Catal. 17 (2001) 363.
[43] A. Iulianelli, A. Basile, Int. J. Hydrogen En. 35 (2010) 3170.
[44] E.Y. Mironova, M.M. Ermilova, N.V. Orekhova, D.N. Muraviev, A.B. Yaroslavtsev, Catal. Today 236 (2014) 64.
[45] F. Borgognoni, S. Tosti, M. Vadrucci, A. Santucci, Int. J. Hydrogen En. 38 (2013) 1430.
[46] Y. Li, W. Ding, X. Jin, J. Yu, X. Hu, Y. Huang, Int. J. Hydrogen En. 40 (2015) 3528.
[47] V. Palma, F. Castaldo, P. Ciambelli, G. Iaquaniello, Clean. Techn. Env. Pol. 14 (2012) 973.